NJC

Accepted Manuscript

This is an *Accepted Manuscript*, which has been through the Royal Society of Chemistry peer review process and has been accepted for publication.

Accepted Manuscripts are published online shortly after acceptance, before technical editing, formatting and proof reading. Using this free service, authors can make their results available to the community, in citable form, before we publish the edited article. We will replace this *Accepted Manuscript* with the edited and formatted *Advance Article* as soon as it is available.

You can find more information about *Accepted Manuscripts* in the Information for Authors.

Please note that technical editing may introduce minor changes to the text and/or graphics, which may alter content. The journal's standard Terms & Conditions and the Ethical guidelines still apply. In no event shall the Royal Society of Chemistry be held responsible for any errors or omissions in this *Accepted Manuscript* or any consequences arising from the use of any information it contains.

ROYAL SOCIETY OF CHEMISTRY

www.rsc.org/njc

NJC

ARTICLE

Effect of Chelating Agent at Different pH on Spectroscopic and Structural Properties of Microwave Derived Hydroxyapatite Nanoparticles: A Bone Mimetic Material

Received 00th November 2015,
Accepted 00th January 2016

DOI: 10.1039/x0xx00000x

www.rsc.org/

Vijay Kumar Mishra[a], Birendra Nath Bhattacharjee[b], Devendra Kumar[b†], Shyam Bahadur Rai[a†], Om Parkash[b]

In the present investigation, the effect of capping agent (EDTA) and pH on optical and structural characteristics of HAp nanoparticles (NPs) have been studied. Six samples of HAp were synthesized under six different chemical conditions. HAp specimens were prepared via microwave irradiation technique (MWIT) in presence and in absence of EDTA at three different pH values 9, 11 and 13. All the samples were calcined at 900 °C. The HAp NPs of different sizes and shapes have been found to be developed. X-ray diffraction (XRD), Scanning Electron Microscopy (SEM) and Transmission Electron Microscopy (TEM) techniques were employed to determine the crystal structure, crystallite size, and bonding parameters of the resulting HAp. The SEM measurements revealed the formation of different morphologies of HAp NPs under different physico-chemical conditions. The electron microscopies revealed that the particle sizes of samples were belonged in the range of ~10-200 nm. TEM results were good agreement with SEM results. The study revealed the vital role of chelating agent (EDTA) playing in the formation of pure phase HAp nanostructures. EDTA assisted the formation of needle-like nanorods of HAP and prevented the agglomeration. EDTA also prevented the carbonate impurities. Carbonate impurities, probably from atmosphere, was observed enough in HAp samples formed without EDTA. Despite the effect of EDTA, the pH of solution also played key role to decide the final morphology of HAp nanostructures. The samples were also characterized spectroscopically by Fourier Transform Infrared (FT-IR) and Raman techniques to understand the molecular interactions. The application of Laser Induced Breakdown Spectroscopy (LIBS) technique detected the presence of N element and confirmed further the formation of HAp powders.

1. Introduction

Hydroxyapatite ($Ca_{10}(PO_4)_6(OH)_2$): HAp was chemically similar to inorganic part of mammalian hard tissues. It has attracted considerable attention of scientists due to its excellent biocompatibility and similarity with natural bone and teeth tissues [1, 2]. HAp has excellent ability to form the chemical bonds to the host bone tissues. It also shows marvelous compatibility with hard tissues as well as skin and other soft tissues of muscles without any toxic effect [3]. Bioactivity of HAp depends on several factors such as morphology of the material, crystal size, Ca/P ratio, presence of ions (carbonate, magnesium, strontium, sodium etc.), morphology and the texture of biomaterial [3, 4]. Since, the clinical applications of HAp were strongly dependent on morphology and crystal size of pure phase HAp hence a considerable attention and efforts are focused now on these factors [5, 6]. Huang et al. (2015) reported Cu-substituted carbonated hydroxyapatite coating, which had good antibacterial efficacy and corrosion resistance with no cytotoxicity [7]. However, Ding et al. (2015) showed the cytocompatibility and corrosion resistance of zinc-doped hydroxyapatite coatings on a titanium substrate [8]. Crystallographic properties and surface morphology of HAp widely depend on preparation routes followed, different resources and starting reagents used and dopants [6, 9]. It was believed that, a suitable morphology having nanoscale size will facilitate the improved applications in different dimensions of bone strengthening, bone healing, osteoporosis, and other bone discussed.

The use of nanostructured HAp as a drug vehicle/carrier in drug delivery/targeted drug delivery/gene delivery/bioimaging etc was one of the latest applications of HAp NPs. It was also reported that, different nanostructures/morphologies of HAp have different drug loading efficiency for a particular drug [10]. Therefore, drug loading efficiency of HAp for a particular drug may be enhanced or controlled by developing a particular nanostructure of HAp. HAp NPs have been widely employed in

[a] Department of Physics, Centre of Advanced Studies, Institute of Science, Banaras Hindu University, 221005, India.
[b] Department of Ceramic Engineering, Indian Institute of Technology, Banaras Hindu University, 221005, India
† Corresponding authors: Tel. +91-542- 6701793, 2307308; Fax: +91-542-2368174, 2369889
Email addresses: devendra.cer@itbhu.ac.in; sbrai49@yahoo.co.in; vijaybioceramic@gmail.com
See DOI: 10.1039/x0xx00000x

delivery systems for antibiotics [11], genes [12, 13] proteins [14] and various drugs [15, 16] due to their excellent biocompatibility and non-toxicity. Recently, Guo et al. (2012) reported the formation of micro and mesoporous carbonated HAp microspheres having good drug loading efficiency and in-vitro investigations of stability of drug [17]. The selection of suitable morphology, size and shape of HAp NPs for an efficient loading of a particular drug used for specific disease was still a challenge for the scientists. Therefore, the development of different nanostructures with a controlled morphology of HAp pure phase was not only desirable but was necessary too. In order to develop various morphologies/ nanostructures of HAp, a lot of efforts were in way. HAp with a slight doping of non reacting metal has been found to affect the morphology of HAp nanostructures drastically [18]. There are several methods, such as sol-gel [19], low temperature synthesis-modified sol-gel technique [20], homogeneous precipitation/co-precipitation [21, 22], hydrothermal [23], mechano-chemical [24], ultrasonic spray freeze-drying [25], Spray dry [26], combustion synthesis [27], Emulsion technique [28], radio frequency plasma spray [29], microwave irradiation technique [30-34] etc have come up in recent years to synthesize HAp. Some biological resources viz. coral skeletal carbonate by hydrothermal exchange [35] and hen's egg shell by precipitation [36] method have also been used to prepare HAp powders. Among these, microwave irradiation technique is found to be very quick, efficient and eco-friendly to prepare pure phase of HAp nanoparticles [37]. Another interesting thing is that the morphology of HAp nanostructures can be controlled easily by suitable microwave power [2] as well as calcination temperatures [30].

A slight change in one or more physical and/or chemical condition(s) in a controlled manner can cause a change in final morphology, crystal size and shape of HAp NPs. Power of the microwave radiation, duration of radiation (microwave on-off working cycle and total microwave exposure time), temperature of synthesis as well as calcinations/annealing/sintering temperature were some of the basic physical parameters which can be tuned to different combinations to control the morphology of HAp nanostructures [2,18,31]. The presence of chelating agent (EDTA, CTAB, etc.), pH value of the solution and initial ingredients (starting reagents) were the chemical parameters which need to be controlled to obtain the desired morphology of HAp NPs.

The present study is focused on the effect of the chemical conditions varying by presence and absence of capping (chelating) agent (EDTA) at different pH values (9, 11 & 13) on final morphology, crystal shape and size of HAp nanostructures derived via microwave irradiation synthesis route. The present study has potential applications in biomedical engineering because; different morphologies with different properties directly affect the bioactivity/biocompatibility/drug loading capacity of HAp on the implantation or administration in host natural soft and hard tissues. Different nanostructures of HAp powders are also useful in bone graft materials, bone cement and coating materials for bone implants.

2. Experimental Procedures

2.1. Sample Preparation

All the chemicals; calcium nitrate tetra hydrate, diammonium hydrogen phosphate and EDTA were purchased from LOBA Chemie of high purity (>99 %) and were used directly without any further purification. Ethylene diamine tetra-acetic acid (EDTA): $C_{10}H_{16}N_2O_8$ served the purpose of capping/complexing agent. In the present investigation, six samples of HAp precursor powders at three different pH values 9, 11 and 13 were prepared via microwave irradiation technique (MWIT). First three samples were prepared in presence of EDTA at pH 9, 11 and 13, however; the other three were prepared without EDTA at the same pHs 9, 11 and 13. The detailed description and procedure for the synthesis of precursor powder at pH 9 followed by Mishra et. al (2014) [30]. The procedure was replicated for pH 11 and 13 controlled by NaOH pellets for rest of the two EDTA assisted samples. The procedure was again replicated for each of pH value by skipping the EDTA. Finally, lime white fine powders called HAp precursor materials at pH 9 was obtained [18]. All the HAp precursor powders were calcined at 900 ºC through a very slow heating rate of 1 ºC/min for the elimination of impurities and formation of fine crystallized HAp. The white color fine powder samples thus obtained were processed for X-ray diffraction and electron microscopy techniques to verify the formation of HAp in nanoscale. Spectroscopic characterizations using FT-IR, Raman and LIBS techniques were then carried out to confirm the formation of HAp.

2.2 Sample Characterizations

In order to investigate the structural and morphological changes occurred in HAp nanoparticles on changing the chemical conditions of preparation, the structural and optical techniques were used. The phase contribution was decided by XRD (Rigaku Desktop Miniflex II X-Ray Diffractometer, equipped with Ni filter and the CuKα radiation). Surface morphologies of nanostructured HAp powders were disclosed by using SEM technique (Inspect S-50, FEI USA (SEA) PTE Ltd., Singapore, FP 2017/12). Transmission Electron Microscopy (TEM, FEI, TECNAI-G^2) with accelerating voltage of 200KV is used. The powder samples were dispersed into the acetone and sonicated for an hour and one drop of this well dispersed suspension is kept upon the carbon coated copper grid. The process was replicated for the other sample. The molecular structures of precursor and other calcined powders were studied by using Fourier Transformed Infrared Spectroscopy (Perkin Elmer spectrum 65, FT-IR) between range 4000-400 cm-1. The samples were diluted by KBr (with materials: KBr was 1:10) to form pellets for IR scanning. FT-IR technique confirmed the formation of HAp in all the samples. LIBS experimental arrangement employed here is shown in (38). It consists of Laser source, a rotational stage (Sandvic Components, India) placed on a jack (Sandvic Components, India) to provide concentric rotation of the sample and the

spectrometer equipped with detector. Nd:YAG laser (532 nm) (continuum surelite III-10) was employed as a laser source having capability of delivering a highest energy of 425 mJ. The pulse duration (FWHM) is 4 ns with maximum pulse repetition rate of 10 Hz. The LIBS spectra of samples were recorded in the spectral range of 200-500 nm on 0.1 nm spectral resolution. Laser pulsed energy was measured by using an energy meter (Genetec-e model UP19K-30H-VM-DO).

3. Results and Discussion

3.1. Spectroscopic Characterizations

3.1.1. Fourier Transform Infrared (FT-IR) Spectroscopy: Fig. 1 (a-f) illustrates the FT-IR spectra of six HAp samples formed under six different physico-chemical conditions. HAp samples (a), (b) and (c), were prepared at three different pH values 9, 11 and 13 respectively in presence of EDTA whereas, samples (d), (e) and (f) were prepared accordingly at the similar pH values 9, 11 and 13 but without using EDTA.

The calcination temperature for all the samples was kept 900 ˚C. All the physical conditions *viz.* power as well as time duration of microwave exposure, on-off working cycle, calcinations temperature and duration (calcinations dynamics) were kept same for all the samples. The IR and Raman active bands observed in these samples are shown along with their assignments in Table 1. IR confirmed the formation of HAp in different physico-chemical conditions. The FT-IR spectra of HAp powders prepared under different conditions show a large number of bands corresponding to different modes of vibrations of various functional groups present. An absorption band observed at 1430 cm^{-1} was weak in the IR patterns (a-c) of the samples formed using EDTA. This band was attributed to v_3 symmetric stretching of carbonate ions (CO_3^{2-}). This band was shifted to 1450 cm^{-1} in the IR spectra (d-f) of samples formed without using EDTA and has strong intensities. Another weak band observed at 1388 cm^{-1} in EDTA assisted as well as without EDTA assisted samples, was due to v_1-symmetric stretching band of carbonate (CO_3^{2-}) impurity.

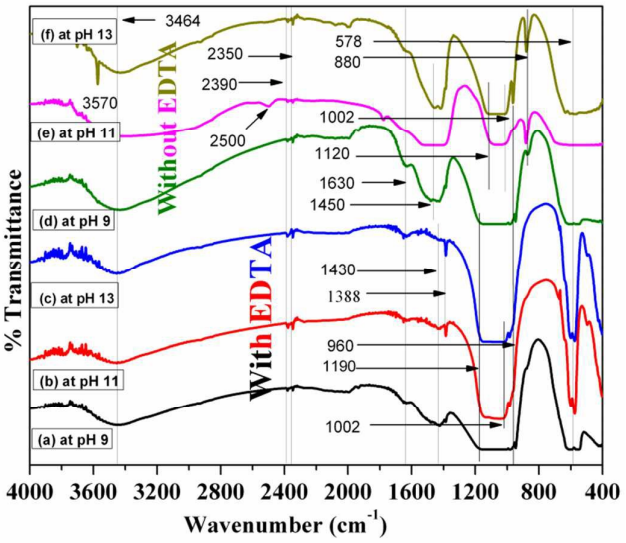

Figure 1: FT-IR spectra of HAp powder samples prepared at pH (a) 9, (b) 11 and (c) 13 with EDTA; and at pH (d) 9, (e) 11 and (f) 13 without EDTA

It was interesting to note that the intensity of this band in the infrared spectra of the samples (a-c) decreases with increase in pH value. However, in the samples (d-f) in which EDTA has not been used, the intensity also increase with pH value of the solution. Two weak but sharp shoulders seen at 2350 and 2390 cm^{-1} in IR spectra of all the samples (a-f) were assigned to v_3-asymmetric stretching of carbonate (CO_3^{2-}) impurity.

The carbonate should not present in pure HAp yet its presence was expected to be due to absorption from atmosphere during sample preparation [39, 40] and so could not be avoided in normal synthesis conditions. However it could be reduced by increasing pH in presence of EDTA. An additional sharp band noticed at 880 cm^{-1} in IR spectra of samples (d-f) formed without EDTA was due to v_2-vibration of carbonate ions. Its intensity increases with the increase of pH of the solution. This band was absent in EDTA assisted HAp v_2-vibration of carbonate ions. This band was absent in EDTA assisted HAp samples. Presence of This additional band due to carbonate impurity in HAp samples formed without using EDTA confirm the superiority of EDTA assisted HAp samples over the samples formed without EDTA. This clearly shows that EDTA prevents the carbonate impurity to be attached during the synthesis. Most plausible reason for this merit of EDTA may be understood on the basis of its complex forming ability. Being a chelating agent, EDTA may have shielded the sites for carbonate ions to be attached. Thus, on the basis of IR studies, we can say that EDTA plays a vital role to form pure phase HAp nanostructures.

Strong absorption bands appearing in between 950-1200 cm^{-1} were the characteristic stretching bands of O-P-O in PO_4^{3-} of HAp. A shoulder noticed at 578 cm^{-1} was assigned to arise due to v_4-asymmetric bending mode of O-P-O. This band was comparatively sharp in (a-c) but appears broad in (d-f) samples, showing again the superiority of EDTA assisted HAp. From these studies, it was concluded that EDTA played an important role in the formation of pure HAp. A strong (characteristic) band at 960 cm^{-1}, noticed in all spectra of HAp samples was attributed to v_1-symmetric stretching mode of P-O in PO_4^{3-}. An envelope between 1002-1120 cm^{-1} preferably in (e) and (f) was attributed to v_3-asymmetric stretching of P-O. Whereas, in the samples (a-d) This spreading was found to be more as 1002-1190 cm^{-1} due to superposition of the band at 1180/1190 cm^{-1}. The broad envelope centered at 3464 cm^{-1} and a weak shoulder at 1630 cm^{-1} were assigned to v_1-stretching and v_2-bending mode of H-O-H (water molecule) respectively present in lattice (30, 31, 40). A sharp shoulder band at 3570 cm^{-1} in IR spectrum (f) was assigned to symmetric stretching mode of the OH^- ions. It was interesting to note that no band due to v-(C-H) stretching mode was seen in the IR spectrum of any of these samples. Absence of v-(C-H) stretching bands between 2800-3000 cm^{-1} in the IR spectra of samples clearly indicates the complete removal of EDTA content from the powder samples (particularly in samples containing EDTA) during washing and rest in the calcination at 900 °C.

Table 1: IR and Raman bands observed in HAp samples (a-c) prepared in presence of EDTA and the samples (d-f) prepared in absence of EDTA at the pH 9, 11 and 13.

FT-IR active bands at wavenumber (cm^{-1})						Raman active bands at wavenumber (cm^{-1})						Assignments Symmetric/Asymmetric bending/stretching
HAp prepared with EDTA at pHs			HAp prepared without EDTA at pHs			HAp prepared with EDTA at pHs			HAp prepared without EDTA at PHs			
(a) 9	(b) 11	(c) 13	(d) 9	(e) 11	(f) 13	(a) 9	(b) 11	(c) 13	(d) 9	(e) 11	(f) 13	
----	----	----	----	----	----	460	----	----	----	----	----	v_2 symmetric bending mode of O-P-O in PO_4^{3-}
578	578	578	578	----	578	----	----	----	----	----	----	v_4 asymmetric bending mode of O-P-O in PO_4^{3-}
----	----	----	880	880	880	----	----	----	----	----	----	v_2 carbonate ions (CO_3^{2-})
960	960	960	960	960	960	965	965	965	965	965	965	v_1 symmetric stretching mode of P-O in PO_4^{3-}
----	1002	1002	----	1002	1002							v_3 asymmetric stretching of P-O in PO_4^{3}
1002-1190	1002-1190	1002-1190	1002-1190	1002-1120	1002-1120	1120	1120	1120	1120	1120	1120	v_3 asymmetric stretching of P-O in PO_4^{3}
----	1388	1388	1388	1388	1388	----	----	----	----	----	----	v_1 symmetric stretching (CO_3^{2-}) vibrational band
1430	1430	1430	1450	1450	1450	----	----	----	----	----	----	v_3 carbonate ions (CO_3^{2-})
1630	1630	1630	1630	1630	1630	----	----	----	----	----	----	v_2 bending mode of H-O-H in lattice H_2O
2350	2350	2350	2350	2350	2350	----	----	----	----	----	----	v_3 asymmetric stretching of carbonate ions (CO_3^{2-})
2390	2390	2390	2390	2390	2390	----	----	----	----	----	----	v_3 asymmetric stretching of carbonate ions (CO_3^{2-})
----	----	----	----	2500	----	----	----	----	----	----	----	Stretching mode of the OH^-
3464	3464	3464	3464	3464	3464	----	----	----	----	----	----	Stretching mode of lattice H_2O
----	----	----	----	----	3570	----	----	----	----	----	----	Symmetric stretching mode of the OH^-

3.1.2. Raman Spectroscopy: Raman spectra of HAp samples formed with and without presence of EDTA at different pH values were shown in Fig. 2 (a-f). Fig. 2 (a-c) show the Raman spectra of HAp samples prepared at pH 9, 11 and 13 in presence of EDTA. However, Fig.2 (d-f) show the Raman spectra of HAp samples formed at pH 9, 11 and 13 in absence of EDTA. A strong peak appearing at 460 cm^{-1} in the Raman profile of sample (a) was assigned to v_2 symmetric bending mode of O-P-O in PO_4^{3-}. This peak does not appear in the Raman spectra of other samples as well as in IR of any sample. A peak noticed at 965 cm^{-1} in all HAp samples (a-f) was attributed to v_1 symmetric stretching mode of P-O in PO_4^{3-}. Intensity of This band decreases in (a-c) with the increase in pH value of the samples. No peak due to carbonate ions was seen in Raman spectra of any of these samples.

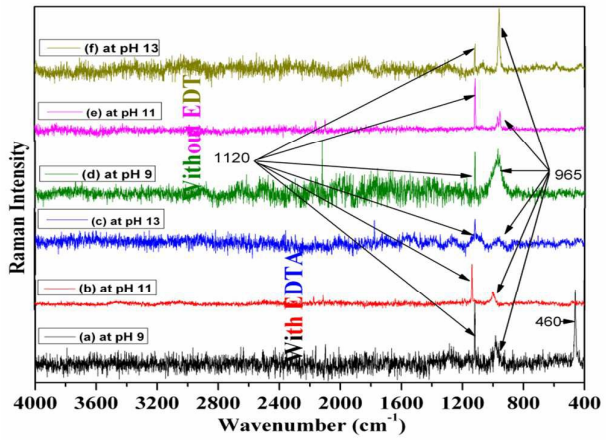

Figure 2: Raman spectra of HAp powder samples prepared at pH (a) 9, (b) 11 and (c) 13 with EDTA; and at pH (d) 9, (e) 11 and (f) 13 without EDTA

A sharp peak at 1120 cm^{-1} appears in Raman spectra of all (a-f) samples and was assigned to v_3 asymmetric stretching vibration of P-O in PO_4^{3-}. The intensities of all the Raman bands decrease with increase in the pH value of final solution. Raman technique confirms again the formation of HAp.

3.1.3. Laser Induced Breakdown Spectroscopy (LIBS): LIBS technique was used to identify the elements present qualitatively in the samples. The samples were taken in pellet form however; any kind of sample (solid, liquid and gas) can be monitored by LIBS. The LIBS spectra of two HAp samples

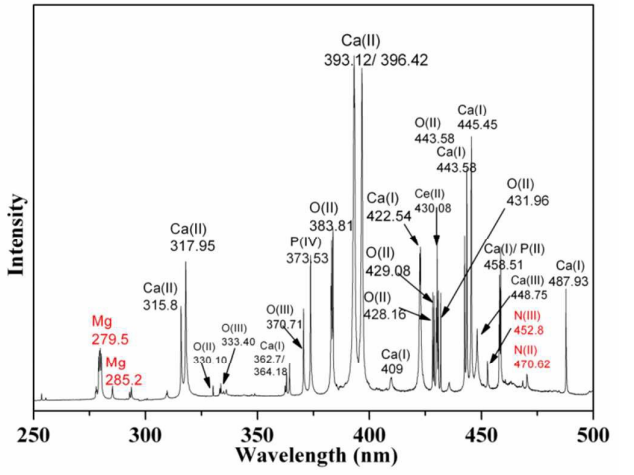

Figure 3: Laser Induced Breakdown Spectrum (LIBS) of HAp powder sample prepared with EDTA at pH 9 and calcined at 900 ºC.

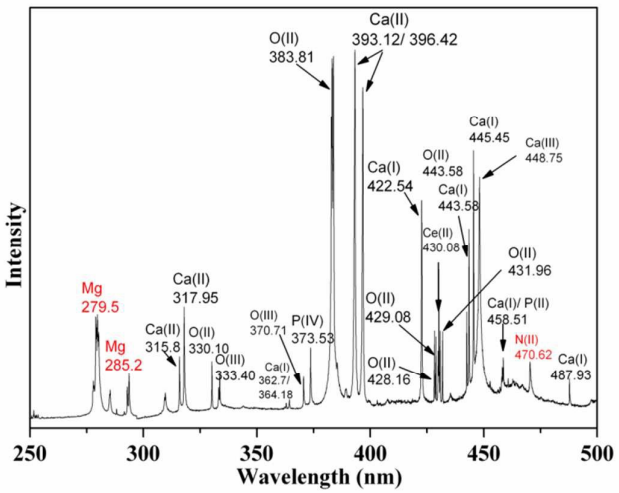

Figure 4: Laser Induced Breakdown Spectrum (LIBS) of HAp powder sample prepared without EDTA at pH 9 and calcined at 900 ºC.

prepared at pH 9 in presence and absence of EDTA and calcined at 900 °C have been studied and samples were shown in Figs. 3 and Fig. 4 respectively. Spectral lines have been identified using the National Institute of Standards and Technology atomic optical database (111- NWAST) [41] and were shown in Table 2.

Table 2: Laser Induced Breakdown Spectral (LIBS) lines with their assignments

LIBS Spectral Line Position (nm)		Assignment
With EDTA	Without EDTA	
279.5	279.5	Mg
285.2	285.2	Mg
315.8	315.8	Ca(II)
317.95	317.95	Ca(II)
330.10	330.10	O(II)
333.40	333.40	O(III)
362.7	362.7	Ca(I)
364.18	364.18	Ca(I)
370.71	370.71	O(III)
373.53	373.53	P(IV)
383.81	383.81	O(II)
393.12	393.12	Ca(II)
396.42	396.42	Ca(II)
409	409	Ca(I)
422.54	422.54	Ca(I)
428.16	428.16	O(II)
429.08	429.08	O(II)
430.08	430.08	Ce(II)
431.96	431.96	O(II)
443.58	443.58	Ca(I)/O(II)
445.45	445.45	Ca(I)
448.75	448.75	Ca(III)
452.8	--------	N(III)
458.51	458.51	Ca(I)/P(II)
470.62	470.62	N(II)
487.93	487.93	Ca(I)

Spectral lines for Ca, P and O have been identified and enlisted in Table 2. These lines show the formation of HAp very clearly. Some Mg as well as N impurity (probably due to chemicals) was also detected by LIBS spectrum. Mg lines at 279.5 and 285.2 were common to both the spectra of HAp derived with EDTA and without EDTA. However, the LIBS pattern of HAp formed with using EDTA contains an additional line for N at 452.8 nm, which may be present either due to chemical impurity or N of EDTA not N of due to presence of EDTA. An EDTA molecule cannot exist at the higher temperatures at which HAp was calcined. A LIBS detects the atom(s) not molecule of impurity. This impurity present at atomic level due to chemicals may not be eliminated easily until we further purify the chemicals after purchasing.

3.2. Structural Characterizations

3.2.1. X-ray Diffraction (XRD) Analysis: X-ray diffraction patterns of all the six HAp samples (a-f), grown in different chemical conditions were shown below in Fig. 5**.** The diffraction patterns (a), (b) and (c), correspond to samples formed at pH 9, 11 and 13 with EDTA respectively whereas, (d), (e) and (f) were without EDTA. A glance on patterns (a) to (f), revealed clearly the formation of hydroxyapatite in all chemical conditions. All the peaks observed in patterns were in good agreement with JCPDS File (24-0033) for Hydroxyalapatite (HAp).

If we compare XRD patterns for the samples (a), (b) and (c) prepared with EDTA at pH 9, 11 and 13, the number of XRD peaks noticed between 25-30 and 50-60 degree in (a) were not seen in (b) and in (c). Moreover as, the pH of HAp precursor solution was increased, the intensity of prominent HAp peaks such as (211) and (230) planes was found to decrease and for the peaks corresponding to (202) and (113) planes were increased remarkably. Peaks due diffraction planes (301) and (102) were observed in pattern (a) and were completely

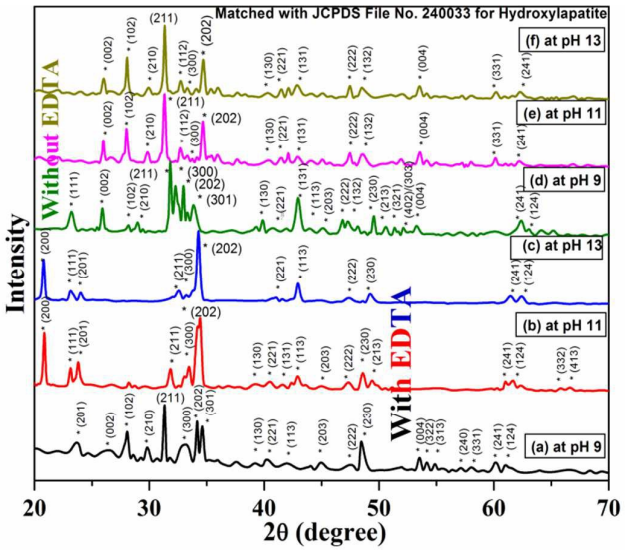

Figure 5: XRD patterns of HAp powder samples prepared at pH (a) 9, (b) 11 and (c) 13 with EDTA; and at pH (d) 9, (e) 11 and (f) 13 without of EDTA

vanished in (b) and (c) as pH was increased. Some new peaks of HAp due to diffraction by planes (200) and (111) started to appear in pattern (b) and become more prominent in (c). Crystallite sizes in these powder samples lie in the range 25-45 nm. On the other hand, the XRD pattern of the samples (d-f) reveal that the peak due to (111) plane appearing in (d) was nearly vanished in (e) and (f). The intensity of peaks due to (002), (131), (300) (230) and (241) also decreases considerably at higher pH values. The peaks due to the planes (200), (201) appearing in EDTA assisted samples were not seen in samples formed without EDTA.

Another interesting feature was that, there was a small peak shift in XRD profiles in EDTA assisted samples. Thus the prominent HAp peaks (211), (300), (202) and (301) in XRD patterns of (a), (b) and (c) samples were found to be slightly shifted towards higher angle side compared to XRD of (d), (e) and (f) patterns. Hike/suppression/appearance/vanishing in the peak intensity may be understood on the basis of atomic structure factor. These changes in the peak intensity occur due to the presence of impurity element(s) in the samples (a-c). Each elements of EDTA contributes the atomic structure factor positive or negative for a particular diffraction plane which affect the peak intensity as well as peak position. The X-ray peak shift may be due to three basic reasons, (i) lattice parameter change, (ii) presence of residual stress and (iii) defect concentration [30, 42]. In the present case, the peak shift seems due to the second reason; presence of residual stress (some impurity element) as nitrogen was revealed also by LIBS technique. Some impurity may not be eliminated even upto 1000 °C. In order to eliminate these, the heat treatment above this temperature is needed. Contribution of nitrogen element positive or negative consequents these peaks shift.

3.2.2. Scanning Electron Microscopy (SEM): Fig.6 (a-d) shows some additional SEM images of four HAp samples prepared under four different physico-chemical conditions. Sample (a) and (b) were the HAp precursor powders prepared using EDTA with pH values 9 and 13 respectively. Images (c) and (d) were the microstructures of samples obtained during calcination of HAp precursor powder (a) at temperatures 600 and 900 °C respectively.

The SEM image of HAp precursor (a) shows needle/strip-like nanostructures. The width of nanostrips formed in HAp precursor (a) was around 50 nm. The HAp powder sample calcined at 600 °C shows almost no change in surface morphology as shown in image (c). It shows needle -like nanostructures of 45 nm width. As shown in micrograph (d), morphology of HAp powder sample was changed drastically on heating at 900 °C. The needle-like nanostructures get converted into capsule-like nanostructures of ~200 nm average diameter on heating at 900 °C. A careful examination of image (c) revealed some flower-like morphology of HAp nanostructures at pH 13 of precursor solution. Some bunches of nanostrips/needles/rods have been found to grow together under applied conditions. These images uncover the effect of pH and calcinations temperature on surface morphology of HAp powders prepared via microwave irradiation technique.

The micrographs (at 1 µm magnification) shown in Fig.7 (a-f) exhibit the simultaneous effect of pH and EDTA (a chelating/capping agent/surfactant) on surface morphology of HAp powders prepared via microwave irradiation route under ambient physico-chemical conditions and calcined at 900 °C. Microstructures (a) to (c) show almost capsules/spheres/ ellipsoids-like homogeneous NPs of HAp grown under calcination at 900 °C.

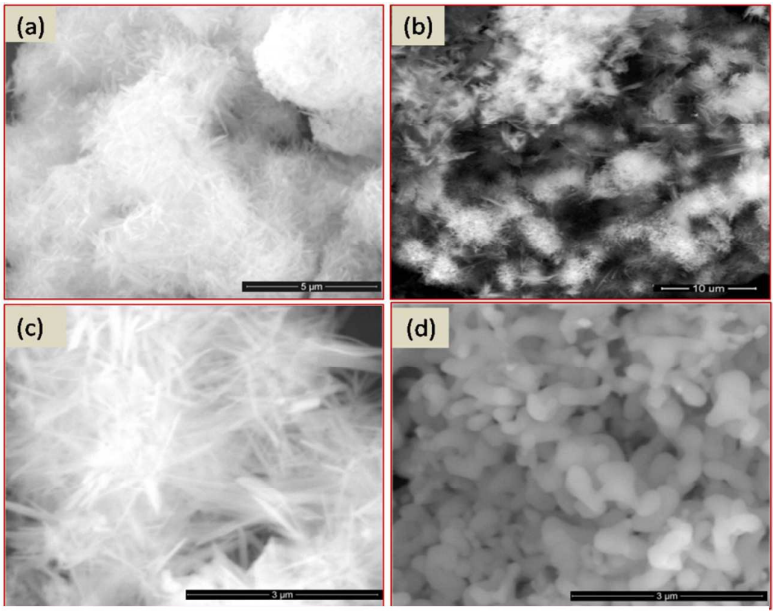

Figure 6: SEM images of HAp precursor powders at pH (a) 9, (b) 13 and HAp powders obtained on calcinations at (c) 600 °C and (d) 900 °C of precursor powder-(a)

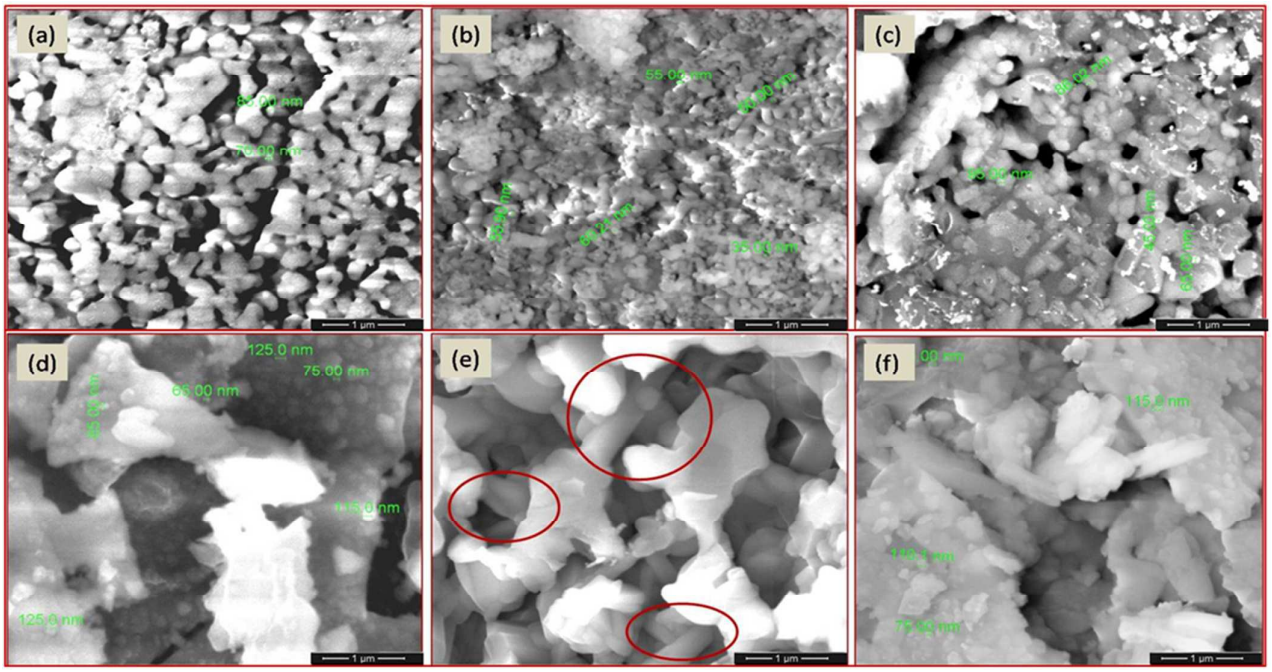

Figure 7: SEM images of HAp powder samples prepared at pH (a) 9, (b) 11 and (c) 13 using EDTA; (d) 9 (e) 11 (f) 13 without EDTA; calcined at 900 °C

Surface morphologies of these samples at their precursor (as synthesized) stage and even up to 600-700 °C show needle/rod-like structure of NPs (see Fig.6 (a and c)). When the samples were calcined at 900 °C the morphologies of samples were totally changed (see Fig.7 (a-f)) Particle sizes of these nanostructures were under 100 nm in sample (a) and (c). However, in sample (b), this value was ~35-60 nm which was much less than (a) and (c). The morphology of this image in (b) was comparatively more homogeneous and dense capsule-like nanostructures similar to as in Fig.6 (d). Images (d), (e) and (f) show the surface morphologies of HAp powders prepared at pH 9, 11 and 13 respectively via microwave irradiation route, without EDTA and calcined at 900 °C. All the physico-chemical conditions of preparation of samples (a-c) were same as in (d-f). From a careful comparison of the image (d and f), we find the size of HAp NPs was around 100 nm and these were strongly embedded into the clusters of several micrometers. The image (e) shows slightly different i.e. rod-like (in rings) microstructures as shown in Fig.7. The diameter of rod-like microstructures was fraction of micrometer and the length may be several micrometers. Effects of EDTA at a certain pH and calcination temperature are obvious and may be understood by Fig.6 (a-d) and corresponding micrographs in Fig.7 (a-c) and (d-f). The particle size in images (d-f) was much larger than article size shown in micrographs (a-c) due to agglomeration of HAp particles. Therefore, we can say that EDTA avoids agglomeration of the particles. Effect of pH on the surface morphology of HAp was clear from Fig.6. Flower-like shapes containing needle/rod/strip-like nanostructures were obtained at higher pH values. The nanorod-like morphology of the HAp calcium phosphate gets converted into capsule like nanostructure due to their diffusion at a temperature near 900 °C. This shows a clear cut effect of calcinations/ annealing/ sintering temperature on the surface morphology of HAp. The detailed study on effect of calcinations/ annealing/ sintering temperatures on the surface morphology of HAp have already been carried out and discussed by Mishra et al (2014) [30].

3.2.3. Transmission Electron Microscopy (TEM): TEM micrographs of the HAp powder samples prepared without using EDTA and using EDTA as capping agent are shown in Fig. 8 (a) and (b) respectively. These both the samples were prepared at same pH 11. A careful examination of microstructures shown in images (a) and (b), one can easily say that the particles formed in both the cases are nanorod like crystals of HAp. However, the size of HAp crystals grown under two different conditions are quite changed. The diameter and length of HAp nanorods like crystals prepared without EDTA are ~ 20 and 200 nm. These dimensions have been found to be less than half for EDTA assisted HAp nanorods. The diameter of the nanorods is ~ 10 nm and length is less than 100 nm. An interesting fact revealed by TEM characterization is that, the nanorods in image (a) are showing *Asparagus* roots like agglomeration marked in dotted yellow ring. However, in (b) micrograph, the nanorods are scattered needle-like separately as marked by several dotted yellow rings. Thus, it is confirmed that the capping agent (EDTA) prevents the agglomeration as also concluded by SEM technique. The results extracted by TEM micrographs are in good agreement with results of SEM microstructures.

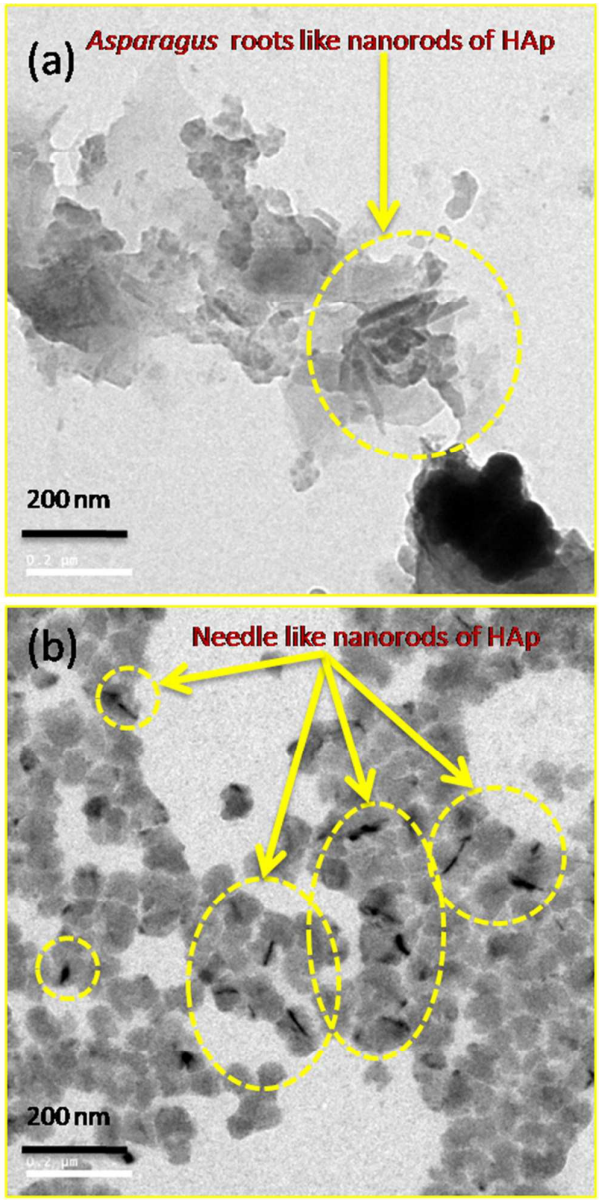

Figure 8: TEM images of HAp powders prepared (a) without EDTA (b) using EDTA

The final morphology of HAp nanomaterial may be understood on the basis of driving force governed by surface energy of particles and surface energy was controlled by physico-chemical conditions. Now, effect of chemical conditions; pH and EDTA on structural and optical characteristics of HAp was discussed below.

A very familiar fact was that when we break a large solid piece of material into smaller parts, it always needs energy to break the bonds between neighboring atoms and it generates new surfaces [43]. The driving force existing in the materials during synthesis was to minimize the surface area. Smaller the surface to volume ratio of the particles, lower was the energy state of the material. In order to minimize the surface energy, the directed bonds in isotropic lattices increase crystallization in rods/ strips or plates i.e. formation of one or two dimensional particles [44].

Solubility of a system depends on the pH value of the solution. Therefore it can affect the chemical precipitation and the particle agglomeration in presence of complexing agent (EDTA). In the beginning the pH of the starting solution was 4. As the pH of the solution was increased, the solubility of the system increases and the solution transferred from milky white color to colorless. At pH 9, the solution became totally transparent and clear. At the initial stages of the experiment (in clear solution before microwave irradiation), a cluster of critical size of HAp would be formed and it forms the nucleus for HAp crystal growth. HAp nuclei grow into crystallites when solution was irradiated by microwaves of frequency 2.45 GHz. The further growth of HAp crystal was controlled totally by stability of Ca-EDTA complex and presence of OH^- on the facets. Due to a poor stability of Ca-EDTA complex at pH 9, Ca^{2+} ions and EDTA get separated from each other. Now due to ionic interaction, surface of OH^- behaves as an active site for absorption of Ca^{2+} ions. In fact at pH 9, there were two opposite facets of crystallite active with OH^- ions and the crystallites grow having an anisotropic structure of HAp under microwave treatment. Consequently, a preferred growth along the (002) axis of hexagonal HAp was observed in X- ray diffraction (XRD) patterns resulting in an increased strip-like/rod-like morphology with larger average particle size [45]. As we increase the pH of the solution, the concentration of OH^- ions and stability of Ca-EDTA complex increases. Therefore Ca^{2+} and EDTA will not be separated from each other. So, Ca and EDTA exist together in the form of Ca-EDTA complex at higher pH values. In these conditions, all the facets of crystallite having high specific surface energy were active at the same potential due to strong adsorption of OH^- ions. These facets have almost equal ability to attach with Ca in form of Ca-EDTA due to almost same concentration of OH^- on each facet. Thus under these physical and chemical conditions, the space between neighboring Ca-EDTA complex molecules resulting an arrangement of Ca atoms in disordered state rather than intrinsic crystal structure of HAp. During the microwave irradiation, the absorbed Ca-EDTA decomposed at appropriate temperature of around 200 $^{\circ}$C. Under homogeneous and fast heating HAp was found to have flower like shape of nanostructure due to anisotropic growth of HAp crystal. It follows that the pH value of final solution and the presence of capping agent (EDTA) play key role in the synthesis of final nanostructure and its shape. Apart from these, the microwave power and duration of on-off cycle also have important roles in the synthesis of nanostructures of HAp.

Though, the chelating agent was desirable but it was not compulsory in the formation of nanostructures of HAp. The template free growth of HAp nanorings having enhanced

properties has been reported [46]. We emphasize that the formation of specific nanostructured morphology in every instance was directly controlled by the driving force and that the surfactants were only incidental for the formation of such structures. Preliminary investigations show that two-dimensional morphologies can be obtained in several other systems including ZnO without using any surfactant. We believe that the primary role of the surfactant was in providing size control in the formation of the two-dimensional structures. However, the role of surfactant was critical for shape-controlled synthesis of various three dimensional morphologies like cubes [47] rods [48], and wires [49]. Roy and co-workers in 1990s synthesized and fabricated the porous and transparent HAp ceramics using microwave processing and sintering [50-52]. It was important to note that the microwave energy corresponding to frequency 2.45 GHz was absorbed strongly by bound water molecules in the hydration sphere of a polyvalent ion. This absorption of microwave power weakens the bonds between the calcium ion and its sphere of hydration, which was of paramount importance for the formation of apatite in aqueous solutions via facilitating the deaquation step [2] though, the solid state synthesis of HAp via microwave route is established already [53].

4. Conclusions

In the present investigations, it is concluded that EDTA and pH play important roles to decide the morphology and structure of HAp. According to IR spectroscopic results, carbonate impurity was absorbed probably from atmosphere in HAp samples during synthesis and it could not be avoided in normal synthesis conditions. However, it can be reduced by using capping agent (EDTA). In present study, EDTA played a vital role to form pure phase HAp nanostructures and prevented incorporation of carbonate impurities. EDTA efficiently affected the morphology of HAp nanostructures. The samples prepared in absence of EDTA show agglomeration of particles. TEM confirmed role of EDTA. TEM exhibited formation of HAP as scattered needle-like nanostructures without agglomeration. The particle size of HAp powder was found to be strongly dependent on the presence of EDTA. The particle size of the EDTA assisted HAp sample (diameter x length is 10 nm x 100 nm) as shown in TEM micrograph (b) was just half of the HAp formed without EDTA (20 nm x 200 nm). Change in pH also caused a large change in morphology of HAp powders. Needle-like nanostructures at pH 9 get reshaped into flower-like at pH 13. By playing with chemical and/or physical preparatory conditions, a desired morphology of HAp structures may be obtained. The HAp nanoparticles of size below 100 nm are extremely useful in specific site as well as normal drug delivery. FT-IR, LIBS, SEM and TEM techniques confirmed the formation of HAp powders. These techniques convinced the superiority of EDTA assisted HAp samples over the samples formed without EDTA.

Acknowledgements

V. K. Mishra is cordially thankful to University Grants Commission, India for financial support in the form of Senior Research Fellowship in Science for Meritorious Students (SRF-UGC-RFSMS) (No. F.5-127/2007 (BSR) 15.03.2013). Authors are thankful to Prof. Ranjan K. Singh for Raman measurements (Department of Physics, Banaras Hindu University), Prof. A. K. Rai (Department of Physics, Allahabad University) for LIBS measurements and Prof. R. K. Mandal (IIT-BHU) for TEM facility.

Notes and references

1 L. L., Hench, *J. Am. Ceram. Soc.*, 1991, **74**, 1487.
2 A. Siddharthan, S. K. Seshadri and T. S. S. Kumar, *Scr. Mater.*, 2006, **55**, 175.
3 W. Suchanek, M. Yashima, M. Kakihana and M. Yoshimura, *Biomater*., 1996, **17**, 1715.
4 S. R. Radin and P. Ducheyne, *J. Biomed. Mater. Res.* 1994, **28**, 1303.
5 J. C. Elliot, *Montpellier: Sauramps Medical, London UK,* 1998.
6 S. Aryal, K.C.R. Bahadur, N. Dharmaraj, K.W. Kim and H.Y. Kim, *Scripta Materialia,* 2006, **54**, 131.
7 Y. Huang, X. Zhang, R. Zhao, H. Mao, Y. Yan and X. Pang, *J. Mater. Sci.* 2015, **50**, 1688.
8 Q. Ding, X. Zhang, Y. Huang, Y. Yan and X. Pang, *J. Mater. Sci.,* 2015, **50**, 189.
9 R. Murugan and S. Ramakrishna, *Cryst. Growth Des*., 2005, **5**, 111.
10 F. Ye, H. Guo and H. Zhang, *Acta Biomater*., 2010, **6**, 2212.
11 Y. Shinto, A. Uchida, F. Korkusuz, N. Araki and K. Ono, *J. Bone Joint Surg*., 1992, **74-B**, 600..
12 S. H. Zhu, B. Y. Huang, K. C. Zhou, S. P. Huang, F. Liu, Y. M. Li, Z. G. Xue and Z. G. Long, *J. Nanopart. Res.,* 2004, **6**, 307..
13 P. Sibilla, A. Sereni, G. Aguiari, M. Banzi, E. Manzati and C. Mischiati, *J. Dent. Res.,* 2006, **85**, 354.
14 S. Dasgupta, A. Bandyopadhyay and S. Bose, *Acta Biomate.,* 2009, **5**, 3112.
15 T.Y. Liu, S.Y. Chen, D.M. Liu and S.C. Liou, *J. Control Release* 2005, **107**, 112.
16 B. Palazzo, M. Iafisco, M. Laforgia, N. Margiotta, G. Natile, C.L. Bianchi, D. Walsh, S. Mann and N. Roveri, *Adv. Funct. Mater.* 2007, **17**, 2180.
17 Y.P. Guo, Y.B. Yao, Y.J. Guo and C.Q. Ning, *Micropor. Mesopor. Mater.,* 2012, **155**, 245.
18 V.K. Mishra, B.N. Bhattacharjee, O. Parkash, D. Kumar and S.B. Rai, *J. Alloys Compd.*, 2014, **614**, 283.
19 G. Bezzi, G. Celotti, E. Landi, T.M.G. L. Torretta, I. Sopyan and A. Tampieri, *Mater. Chem. Phys.,* 2003, **78**, 816.
20 S. Jadalannagari, S. More, M. Kowshik and S. R. Ramanan, *Mater. Sci. Eng. C*, 2011, **31**, 1534
21 H. Zhang, S. Li and Y. Yan, *Ceram. Int.*, 2001, **27**, 451.
22 L.B. Kong, J. Ma and F. Boey, *J. Mater. Sci.*, 2002, **7**, 1131.
23 H.S. Liu, T.S. Chin, L.S. Lai, S.Y. Chiu, K.H. Chuang, C.S. Chang and M.T. Lui, *Ceram. Int.*, 1997, **23**, 19.
24 M. Toriyama, A. Ravaglioli, A. Krajewski, G. Celotti and A. Piancastelli, *J. Eur. Ceram. Soc.,* 1996, **16**, 429.
25 K. Itatani, K. Iwafune, F.S. Howell and M. Aizawa, *Mater. Res. Bull.*, 2000, **35**, 575.
26 P. Luo and T.G. Nieh, *Mater. Sci. Eng. C*, 1995, **3**, 75.
27 A. C. Tas, *J. Eur. Ceram. Soc.,* 2000, **20**, 2389.
28 S. Bose and S.K. Saha, *Chem. Mater*., 2003, **15**, 4464.

29 M. Roy, A. Bandyopadhyay and S. Bose, *J. Am. Ceram. Soc.,* 2010, **93**, 3720.
30 V.K. Mishra, S.B. Rai, B.P. Asthana, O. Parkash and D. Kumar, *Ceram. Int.,* 2014, **40**, 11319.
31 V.K. Mishra, S.K. Srivastava, B.P. Asthana and D. Kumar, *J. Am. Ceram. Soc.*, 2012, **95**, 2709.
32 J. Liu, K. Li, H. Wang, M. Zhu and H. Yan, *Chem. Phys. Lett.,* 2004, **396**, 429.
33 A. Lak, M. Mazloumi, M.S. Mohajerani, S. Zanganeh, M.R. Shayegh, A Kajbafvala, H. Arami and S.K. Sadrnezhaad, *J. Am. Ceram. Soc.*, 2008, **91**, 3580.
34 N.Y. Hsu and Y.W. Lin, *New Journal of Chemistry*, 2015, DOI: 10.1039/c5nj02263k
35 D. M. Roy and S. K. Linnehan, *Nature* 1974, **247**, 220.
36 D.L. Goloshchapov, V.M. Kashkarov, N.A. Rumyantseva, P.V. Seredinn, A.S. Lenshin, B.L. Agapov and E.P. Domashevskaya, *Ceram. Int.,* 2013, **39**, 4539
37 H. Monma and T.J. Kamiya, *Mater. Sci.*, 1987, **22**, 4247.
38 G.S. Maurya, A. Jyotsana, R. Kumar, A. Kumar and A.K. Rai, *Phys. Scr.,* 2014, **89**, 075601.
39 N. Ignjatovic, V. Savich, S. Najman, M. Plavsic and D. Uskokovic, *Biomaterials*, 2001, **22**, 571.
40 L. Li, Y. Liu, J. Tao, M. Zhang, H. Pan, X. Xu and R. Tang, *J. Phys. Chem. C,* 2008, **112**, 12219.
41 National Institute of Standards and Technology, "Electronic database," http://physics.nist.gov/PhysRefData/ASD/lines form.html.
42 Z.E. Erkmen, *J. Biomed. Mater. Res. B,* 1999, **48**, 861.
43 D. Vollath, Nanomaterials: An introduction to synthesis, properties and applications, WILEY-VCH Verlag GmbH and Co. KGaA: Weinheim- Germany, 2008.
44 H. Cao, L. Zhang, H. Zheng and Z. Wang, *J. Phys. Chem. C*, 2010, **114**, 18352.
45 E.S. Ahn, N.J. Gleason, A. Nakahira and J.Y. Ying, *Nano Lett.,* 2001, **1**, 149.
46 A.J. Nathanael, S.I. Hong, D. Mangalaraj, N. Ponpandian and P.C. Chen, *Cryst. Growth Des*., 2012, **12**, 3565.
47 Y. Sun and Y. Xia, *Sci.*, 2002, **298**, 2176.
48 Murphy, J. Catherine and N.R. Jana, *Adv. Mater.,* 2002, **14**, 80.
49 A. Halder and N. Ravishankar, *Adv. Mater.,* 2007, **19**, 1854.
50 Y. Fang, D.K. Agrawal, D.M. Roy and R. Roy, *J. Mater. Res.,* 1992, **7**, 490.
51 Y. Fang, D.K. Agrawal, D.M. Roy and R. Roy, *J. Mater. Res.,* 1994, **9**,180.
52 Y. Fang, D.K. Agrawal, D.M. Roy and R. Roy, *Mater. Lett.,* 1995, **23**, 147.
53 J.M. Cao, J. Feng, S.G. Deng, X. Chang, J. Wang, J.S. Liu, P. Lu, H.X. Lu, M.B. Zheng, F. Zhang, and J. Tao, J. Mater. Sci., 2005, 40, 6311.

TOC ENTRY

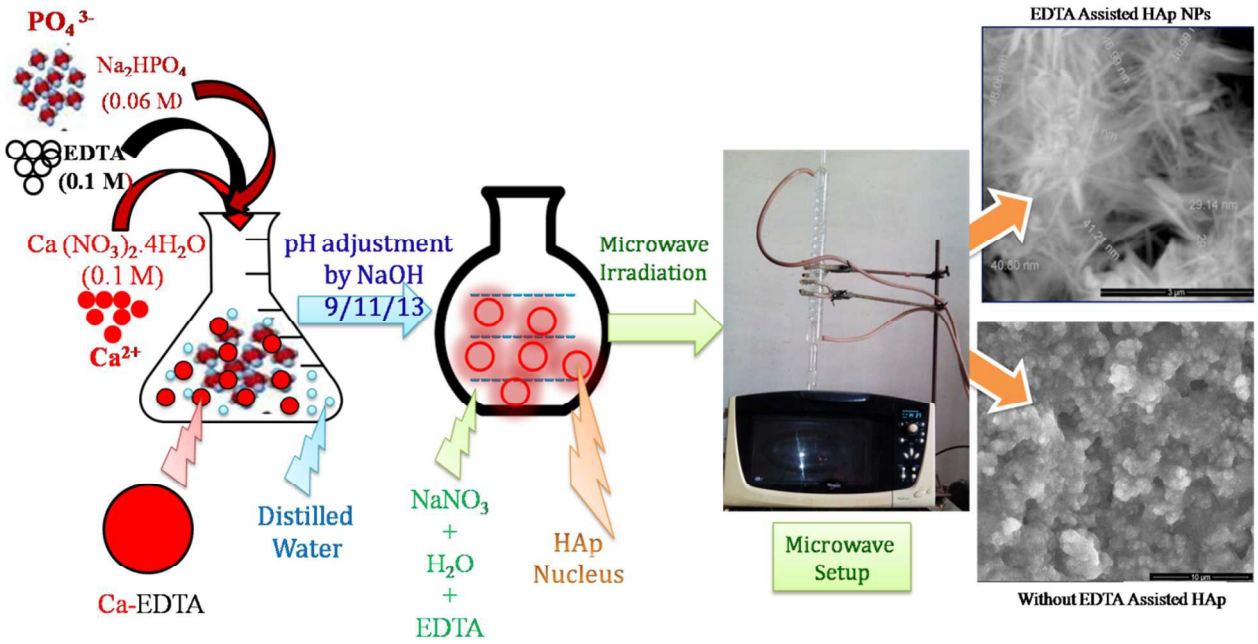

Graphical Abstract

Research Highlights

Asparagus root-like and scattered needle-like formation of hydroxyapatite nanoparticles under microwave irradiation